

# Microstructural Evolution of the 55 Wt Pct Al-Zn Coating During Press Hardening

CHANG WOOK LEE and BRUNO CHARLES DE COOMAN

Press hardening is increasingly being used to produce ultra-high strength steel parts for passenger cars. Al-Si, Zn, and Zn-alloy coatings have been used to provide corrosion protection to press hardening steel grades. The use of coatings has drawbacks such as coating delamination or liquid metal-induced embrittlement. In the present work, the microstructural evolution of Al-Zn coating during press hardening was studied. The 55 wt pct Al-Zn coating can in principle provide both Al barrier protection and Zn cathodic protection to press hardened steel. During the heat treatment associated with the press hardening, the 55 wt pct Al-Zn alloy coating is converted to an intermetallic surface layer of  $\text{Fe}_2\text{Al}_5$  and a FeAl intermetallic diffusion layer. The Zn is separated from both intermetallic compounds and accumulates at grain boundaries and at the surface. This Zn separation process is beneficial in terms of providing cathodic protection to Al-Zn coated press hardening steel.

DOI: 10.1007/s11661-014-2362-6

© The Minerals, Metals & Materials Society and ASM International 2014

## I. INTRODUCTION

CONTRIBUTING to light-weighting passenger vehicles has become a critical issue for the steel industry. Ultra-high strength steels have been developed to address this requirement from the automotive industry, allowing for the design of the vehicles with high mileage, less greenhouse gas emission, and an enhanced passive safety in vehicle collision situations.<sup>[1,2]</sup> To satisfy fuel efficiency requirements, CO<sub>2</sub>-emissions regulations and customer demands, the most cost-effective method is the increased use of high strength steel in car body manufacturing, as it makes it possible to reduce the mass of passenger car without loss of mechanical properties.<sup>[3]</sup> The use of higher strength materials makes most forming process more difficult as it requires higher forming forces and often results in forming defects related to excessive spring back.<sup>[4]</sup>

The press-hardening process was originally developed and patented by the Plannja Company to produce ultra-high strength steel parts by the simultaneous forming of the soft metal at high temperature and the quenching effect of water-cooled forming dies.<sup>[5,6]</sup> In the press-hardening process, the press-hardenable steel (PHS) sheet is heated to the austenite stability temperature range. The high temperature fully austenitic microstructure is relatively soft and it can be formed much more easily than martensite at room temperature. During the combined die-quenching heat treatment and forming

process, the steel sheet is quenched to room temperature and a fully martensitic microstructure is obtained with a tensile strength of approximately 1500 MPa.<sup>[7]</sup> Press-hardened steel sheets are currently being used in structural parts in the body-in-white of passenger cars for the A-pillar, B-pillar, bumper, and roof rail.<sup>[5]</sup>

In the development stages of press hardening technology, bare steel was utilized. Chromium shot blasting was used for the removal of the iron oxide scale. Due to the requirement of corrosion resistance, a number of different coatings have been developed for press hardening steel. The Al-10 pct Si aluminized coating is currently the most widely used coating.<sup>[8]</sup> The Al-10 pct Si alloy coating provides a very good barrier protection and it efficiently suppresses decarburization and surface oxidation during the press-hardening process. During the heat treatment, various Fe-Al intermetallic compounds are formed; this avoids the melting of the coating because the intermetallic Fe-Al phases have a high melting temperature.<sup>[5,9]</sup> However, aluminized coatings do not provide sufficient ductility for press hardening.<sup>[10]</sup> An aluminide coating has been proposed to improve coating ductility. It is obtained by a diffusion annealing of the Al-10 pct Si alloy coating.<sup>[10,11]</sup> Al-based coatings provide cathodic corrosion resistance as well.<sup>[12]</sup> However, it provides a relatively lower sacrificial effect on steel than the Zn and Zn-alloy coatings. Zn and Zn-alloy coatings have therefore been developed to provide cathodic corrosion protection to PHS grades. The use of Zn and Zn-alloy coatings for press hardening has proven to be challenging due to their low melting temperature and the ease of evaporation of the Zn. Hot-dip galvanizing of PHS with Al-added Zn has the advantage to suppress Zn evaporation at high temperature.<sup>[13]</sup> Liquid Zn may cause liquid metal-induced embrittlement (LMIE).<sup>[14]</sup> Microcracks also occur in areas of high friction between the steel sheet and the tools.<sup>[15]</sup> After the press-hardening

---

CHANG WOOK LEE, Graduate Student, is with the Graduate Institute of Ferrous Metallurgy, Pohang University of Science and Technology, Pohang, South Korea. BRUNO CHARLES DE COOMAN, Professor, is with the Graduate Institute of Ferrous Metallurgy, Pohang University of Science and Technology, and also Director, with the Materials Design Laboratory, Pohang University of Science and Technology. Contact e-mail: decooman@postech.ac.kr

Manuscript submitted February 6, 2014.

Article published online May 24, 2014

process, the weldability is deteriorated due to the presence of Zn-oxide formation on the surface. As Zn oxide increases the contact resistance, it must be removed by abrasive blasting.<sup>[16]</sup>

In this contribution, the 55 wt pct Al-Zn coating, also known as Galvalume<sup>®</sup>, was applied on a PHS. The hot-dip 55 wt pct Al-Zn coating has been developed to benefit from the combined barrier action of Al and the cathodic protection of Zn. The purpose of this paper is to report the results of a study of the microstructural evolution of 55 wt pct Al-Zn coating during the heat treatment associated with the press-hardening process.

## II. EXPERIMENTAL

A 22MnB5 (Fe-0.19 pct C-1.3 pct Mn-0.002 pct B in mass pct) PHS grade was prepared by vacuum induction melting (VIM) and the ingots were hot rolled prior to cold rolling to a final thickness of 1.5 mm. The full hard cold-rolled panels were hot-dip coated with a 55 wt pct Al-Zn alloy coating in a laboratory hot-dip coating simulator. The temperature of the 55 wt pct Al-Zn bath, which contained 1.6 wt pct Si, was kept at 953 K (680 °C), and the dipping time was fixed at 5 seconds. The thickness of 55 wt pct Al-Zn coating was about 17  $\mu\text{m}$ . The samples were heated to a peak temperature in the range of 973 K to 1173 K (600 °C to 900 °C) in a furnace using a heating rate of 5 K s<sup>-1</sup>, to characterize the coating layer microstructural evolution and the coating/steel interdiffusion. After isothermal holding, the samples were die-quenched to room temperature with cooling rate about -70 K s<sup>-1</sup> to obtain a lath martensite microstructure in the steel matrix. The total heating time was kept fixed at 6 minutes. To investigate the effect of annealing time on the 55 wt pct Al-Zn coating during the heat treatment, two additional heat treatment conditions were used, with a total heating time of 4 and 8 minutes at 1173 K (900 °C).

After the tests, samples of the heat-treated steels were cold-mounted in a polymer resin. After polishing with an alcohol-based diamond suspension, the surface of the samples was gold-coated by physical vapor deposition (PVD) to improve the surface-conductivity. The specimens were observed in a ZEISS Ultra 55 Field Emission Scanning Electron Microscopy (FE-SEM) operated at 15 kV and analyzed by Energy Dispersive Spectroscopy (EDS). The specimens were also observed in a JEOL JXA-8530F Field Emission Electron Probe Micro-Analyzer (FE-EPMA) operated at 15 kV and analyzed by Wavelength Dispersive Spectroscopy (WDS) for the elemental mapping of Zn in the diffusion layer. Transmission Electron Microscopy (TEM) samples were prepared by the focussed ion-beam thinning method in a FEI QUANTA 3D. The microstructural analysis was carried out in a JEOL JEM-2100F Field Emission Transmission Electron Microscopy (FE-TEM) operated at 200 kV and the samples were analyzed by Energy Dispersive Spectroscopy (EDS).

Samples of uncoated and Zn-coated 22MnB5 steel were used as to evaluate the cathodic protection properties of the 55 wt pct Al-Zn coating. For the

preparation of the Zn-coated 22MnB5 PHS, the temperature of the Zn-0.12 mass pct Al hot-dip galvanizing bath was 723 K (450 °C), and the dipping time was 5 seconds. The thickness of the hot-dip Zn coating was about 10  $\mu\text{m}$ . The corrosion properties of the 55 wt pct Al-Zn coating were measured before and after the heat treatment at 1173 K (900 °C) by potentiodynamic polarization tests in a 3 wt pct NaCl solution. The tests were carried out with a PAR Electrochemical Workstation VersaSTAT3, with a platinum counter electrode and a standard calomel electrode. The potentiodynamic polarization tests were carried out by sweeping the potential from -250 mV (*vs* open circuit potential) to 500 mV (*vs* SCE) at a scan rate of 0.167 mV s<sup>-1</sup>.

## III. RESULTS

Figure 1 shows a cross-sectional micrograph and the elemental concentration profile of the hot-dip 55 wt pct Al-Zn coated 22MnB5 before heat treatment. The coating was composed of a Zn-rich and an Al-rich solid solution. Point 1 in Figure 1 indicates a Zn-rich region, with a Zn content of 63.5 wt pct. Point 2 in Figure 1 corresponds to an Al-rich region, with an Al content of 65 wt pct. The depth profile also confirmed the presence of these two distinct regions in the coating layer. An alloy layer was formed at the interface between the steel substrate and the Al-Zn coating layer. Its thickness was 2  $\mu\text{m}$ . The chemical composition of the intermetallic alloy layer is listed in Table I. The chemical composition of this interfacial layer has been reported in the literature and corresponds to the T<sub>5C</sub> phase.<sup>[17]</sup> It contains Si which is known to control the reaction between the molten Al-Zn alloy coating and the steel substrate by formation of a solid interfacial layer which acts as an inhibition layer suppressing the formation of Fe-Al intermetallic compounds during the hot-dipping process.<sup>[17,18]</sup> The Zn-Al phase diagram shows that the 55 wt pct Al-Zn coating becomes partially liquid at 763 K (490 °C) and is fully liquid at 843 K (570 °C). The coating is fully liquid if no intermetallic compounds with a high melting temperature are formed during the press hardening heat treatment.<sup>[19]</sup>

Figure 2 shows a cross-sectional micrograph and the corresponding EDS depth profile of specimens which were heat treated isothermally in the 873 K to 1173 K (600 °C to 900 °C) temperature range. At 873 K (600 °C), no significant changes were observed in the microstructure of the original coating and the elemental distribution was similar to the one in the initial microstructure.

For the specimens heat treated at temperatures higher than 973 K (700 °C), the microstructure of the coating was clearly altered. A globular-shaped Al-rich phase developed which was surrounded by a Zn-rich phase much richer in Zn (84.8 wt pct) than at 700 °C (63.5 wt pct). The thickness of the alloy layer increased to 5  $\mu\text{m}$ . According to the Al-Zn phase diagram (Figure 1), the coating is expected to be fully liquid in the 873 K to 973 K (600 °C to 700 °C) temperature

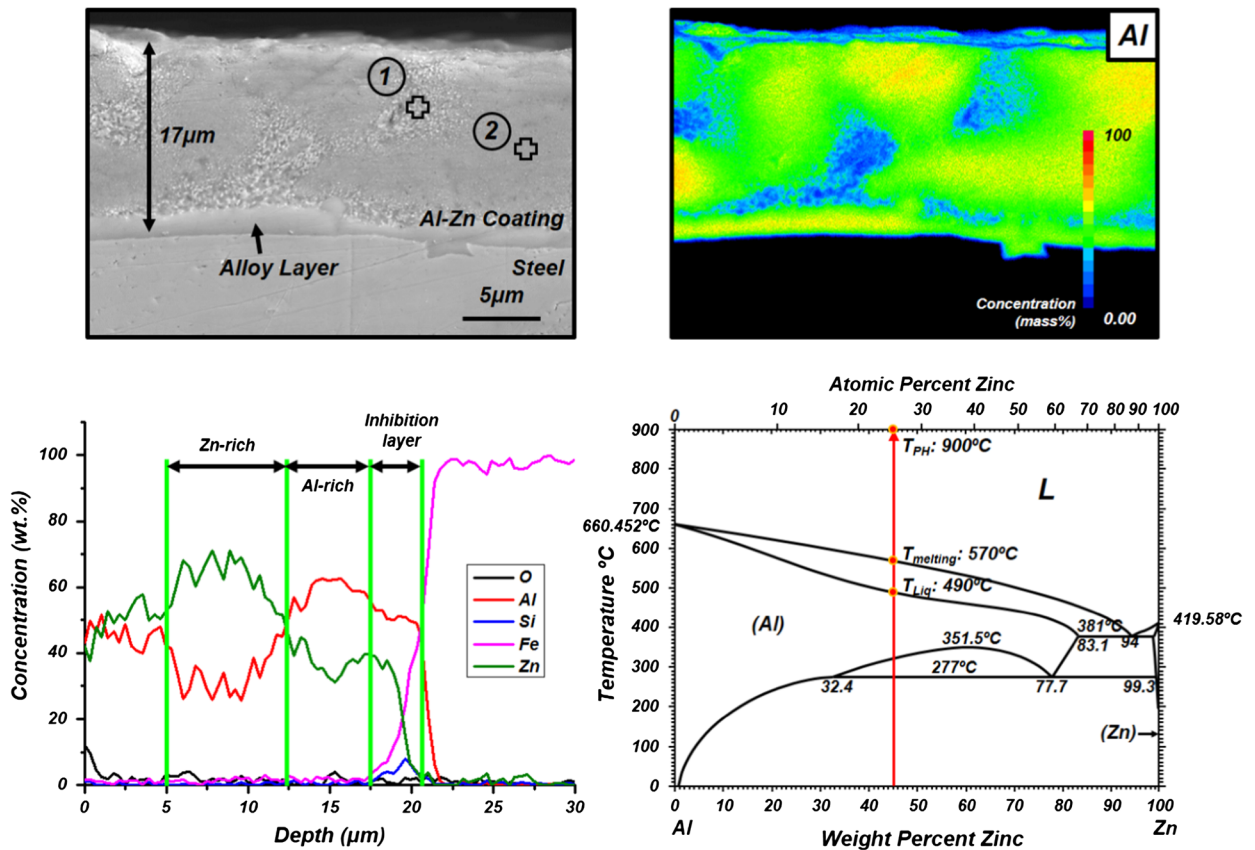


Fig. 1—(Top) Cross-sectional SEM micrograph and corresponding elemental mapping for Al. (Below) Surface depth profile of 55 wt pct Al-Zn coated 22MnB5 prior to the press hardening heat treatment. Zn-Al phase diagram.<sup>[19]</sup>

Table I. EDS Analysis of the Intermetallic Alloy Layer

Position	Al (Wt Pct)	Si (Wt Pct)	Fe (Wt Pct)	Zn (Wt Pct)
Top	51.9	8.4	24.7	15.0
Middle	50.9	6.6	35.7	6.8
Bottom	50.0	3.6	42.3	4.1

range during the heat treatment if no Fe diffusion into the coating takes place and if no Fe-Al intermetallic compounds are formed. The alloy layer remains in the solid state because of the high melting temperature of the Fe-Al intermetallic compounds. At 1023 K (750 °C), the total thickness of the coating had decreased considerably, and the entire coating was composed of two Fe-Al intermetallic compound layers. The first alloy layer, close to the steel, occupied close to half the original total coating layer. It was identified as Fe<sub>2</sub>Al<sub>5</sub> by means of EDS analysis. At higher temperatures, Fe atoms diffused into the coating beyond the alloy layer and reacted with the coating. In the process, the Fe-Al intermetallic compound FeAl<sub>3</sub> was formed. In addition, a thin layer of a Zn-rich phase was formed. At 1083 K (810 °C), the original coating layer was almost entirely composed of the Fe<sub>2</sub>Al<sub>5</sub> intermetallic compound containing 40.2 wt pct Fe, 43.7 wt pct Al, 1.0 wt pct Si, and 15.1 wt pct Zn. A Zn-rich phase was also present; it was visible as a light gray phase in Figure 2. This Zn-rich

phase was encapsulated between the globular-shaped FeAl<sub>3</sub> grains in the surface alloy layer. In the sample heated to 1173 K (900 °C), the depth profile clearly showed that the Zn and the O concentrations were very high on the top surface, indicating the formation of an outer ZnO layer. Multiple voids were formed in the coating which contained mainly the Zn-rich phase, the Al having diffused into the steel substrate, as indicated by the Al diffusion profile shown in Figure 2. The Al diffusion depth into the steel substrate was about 15 μm. Cracks were present in the diffusion layer even though there was no deformation during the heat treatment. Figure 3 shows isothermal sections of the ternary Fe-Al-Zn phase diagram in the temperature range of 873 K to 1173 K (600 °C to 900 °C) calculated by means of the Factsage equilibrium thermodynamics computational software. The compositions obtained from the EDS depth profiles shown in Figure 2 were superimposed on the equilibrium phase diagram. These ternary phase diagrams clearly illustrate that the thermal treatment

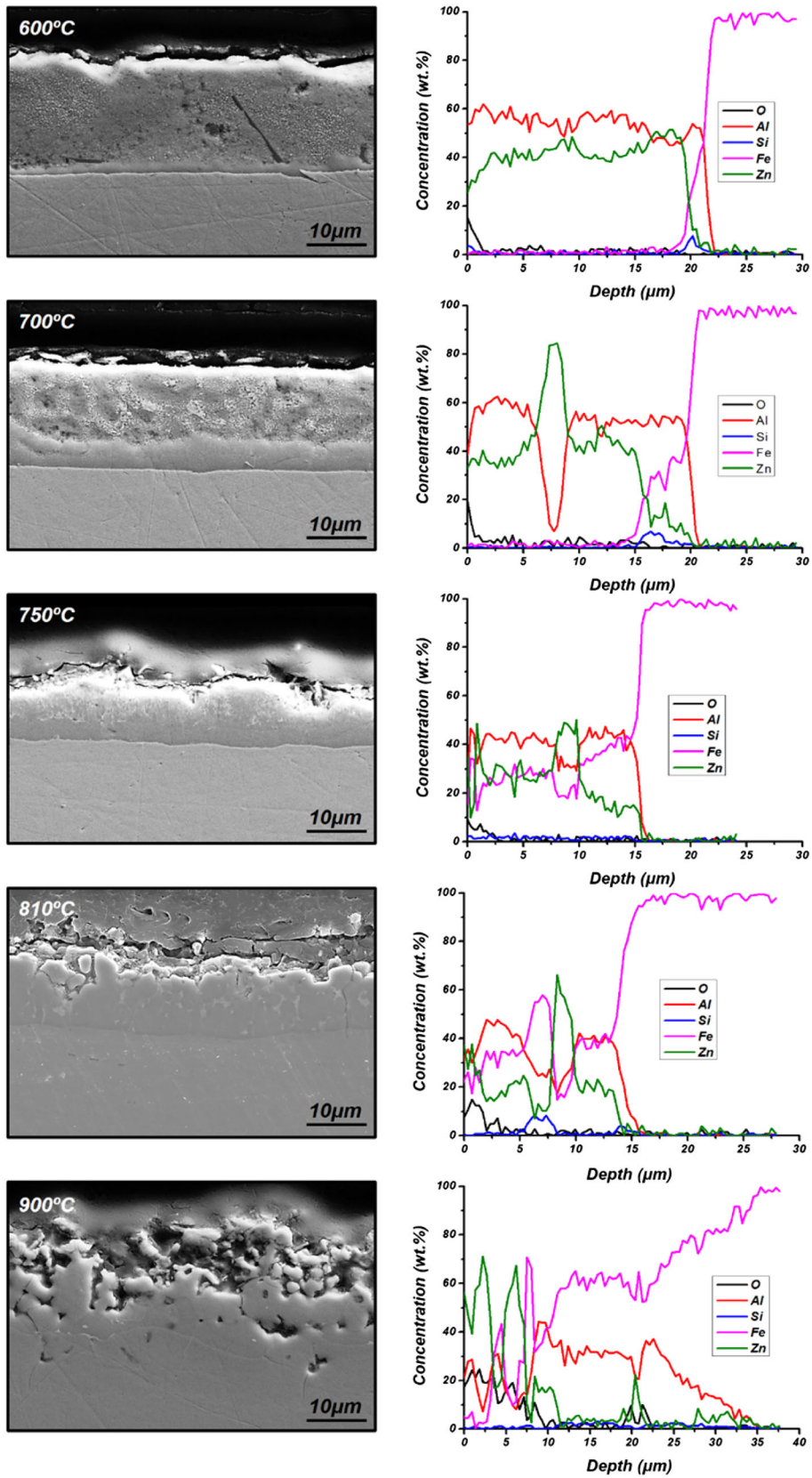


Fig. 2—SEM micrographs and corresponding elemental depth profiles of 55 wt pct Al-Zn coated 22MnB5 PHS heat treated in the temperature range 873 K to 1173 K (600 °C to 900 °C).

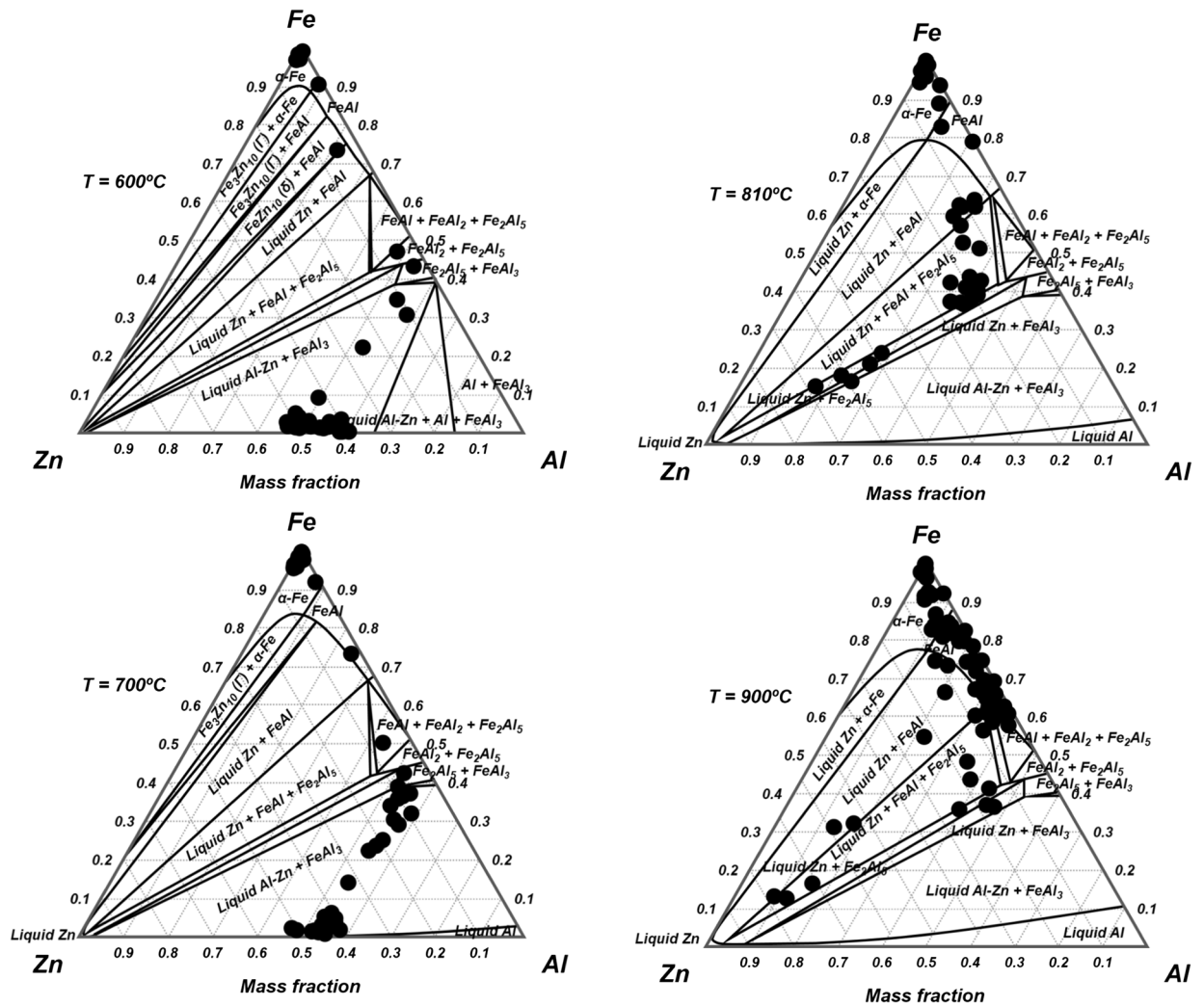


Fig. 3—Combination of the experimentally determined coating composition and the isothermal sections of the ternary Fe-Al-Zn phase diagram in the temperature range 873 K to 1173 K (600 °C to 900 °C) calculated by Factsage.

leads to the preferred formation of Fe-Al intermetallic compounds, and that the formation of Fe-Zn intermetallic phases was fully suppressed during the heat treatment.

Figure 4 shows a bright-field TEM micrograph and the corresponding selected area diffraction patterns for the intermetallic phases formed in a specimen heat treated at 1023 K (750 °C). The TEM sample was extracted using the focused ion-beam (FIB) milling technique, from the interface between the Al-Zn coating layer and the alloy layer. The Fe-Al intermetallic phases were identified by means of electron diffraction. The top layer was identified as FeAl<sub>3</sub> and the lower layer was Fe<sub>2</sub>Al<sub>5</sub>. The grain size of the FeAl<sub>3</sub> phase was much smaller than the grain size of the Fe<sub>2</sub>Al<sub>5</sub> phase. Figure 5 shows a STEM micrograph of the same specimen together with the chemical analysis obtained by EDS. The chemical composition of the coating was also found to correspond to FeAl<sub>3</sub> and Fe<sub>2</sub>Al<sub>5</sub>. The micrograph and the associated Zn elemental distribution obtained by EDS, clearly shows that the grain boundaries of the

Fe-Al intermetallic compounds contain a high Zn concentration compared to the Zn concentration in the matrix of the Fe-Al intermetallic compounds. Figure 6 shows a bright-field TEM micrograph and the corresponding diffraction patterns of the specimen heat treated at 1173 K (900 °C). The FIB TEM sample was extracted from the interface between the alloy layer and the diffusion layer. The alloy layer was identified as Fe<sub>2</sub>Al<sub>5</sub>, and the diffusion layer was identified as FeAl by means of diffraction pattern analysis. Figure 7 shows a STEM micrograph and the Al composition distribution obtained by EDS. The analysis of the points 1-3 confirmed that the alloy layer was Fe<sub>2</sub>Al<sub>5</sub>. The compositions of the points 4 and 5 were extremely high in Zn, indicating that the grain boundaries of the Fe-Al intermetallic compound contained Zn, which was liquid at 1173 K (900 °C). This liquid Zn also penetrated into the grain boundaries of the diffusion layer. The analysis of point 7 located in a grain boundary of the diffusion layer had a much higher Zn content than the grain boundary of the diffusion layer (Point 6). The diffusion

layer was composed of the ordered B2 FeAl intermetallic phase which was formed between the alloy layer and the matrix  $\alpha$ -Fe phase with Al in solid solution.

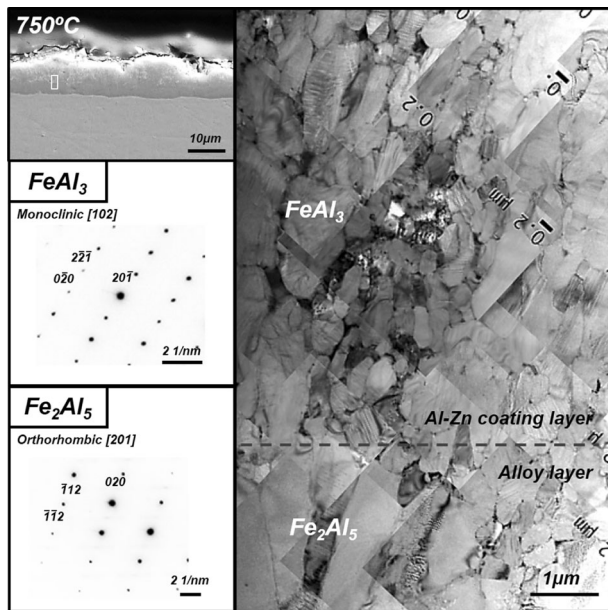


Fig. 4—TEM micrograph and corresponding selected area diffraction patterns for the  $\text{FeAl}_3$  and  $\text{Fe}_2\text{Al}_5$  intermetallic phases in 55 wt pct Al-Zn coated 22MnB5 PHS heat treated at 1023 K (750 °C).

#### IV. DISCUSSION

The interaction between Al and Zn atoms is weak and there are no known intermetallic phases between Al and Zn. This also explains why the solubility of Zn in Al is very large. In contrast, Fe forms several very stable intermetallic phases with Al during the interdiffusion taking place during the press hardening heat treatment. These Fe-Al intermetallics have a very low Zn solubility. Zn was, therefore, expelled for the Fe-Al intermetallic phases into the inter-granular region, and accumulated at the grain boundaries in the Fe-Al intermetallic compounds. The presence of the metallic Zn is beneficial in terms of providing cathodic protection to PHS. The heat-treated 55 wt pct Al-Zn alloy layer may therefore have a higher corrosion resistance than a galvanized-coated PHS after the press hardening heat treatment as a galvanized coating is mostly converted to a  $\Gamma$  phase layer and  $\alpha$ -Fe(Zn) during press hardening. The  $\Gamma$  phase has a lower Zn content, about 70 wt pct, than pure Zn.<sup>[14]</sup>

As the pure Zn phase has a low melting temperature of 692 K (419 °C), it is present as a liquid and it can penetrate *via* the grain boundaries in the  $\text{Fe}_2\text{Al}_5$  alloy layer into the FeAl diffusion layer. This may eventually lead to the LMIE of a PHS part when stress is applied during the press forming.

Figure 8 shows cross-sectional images and the elemental Zn distribution at the surface of PHS specimens heat treated at 1143 K and 1173 K (870 °C and 900 °C). Three areas had a high Zn concentration: (a) The Zn-oxide layer on the top surface, (b) the grain

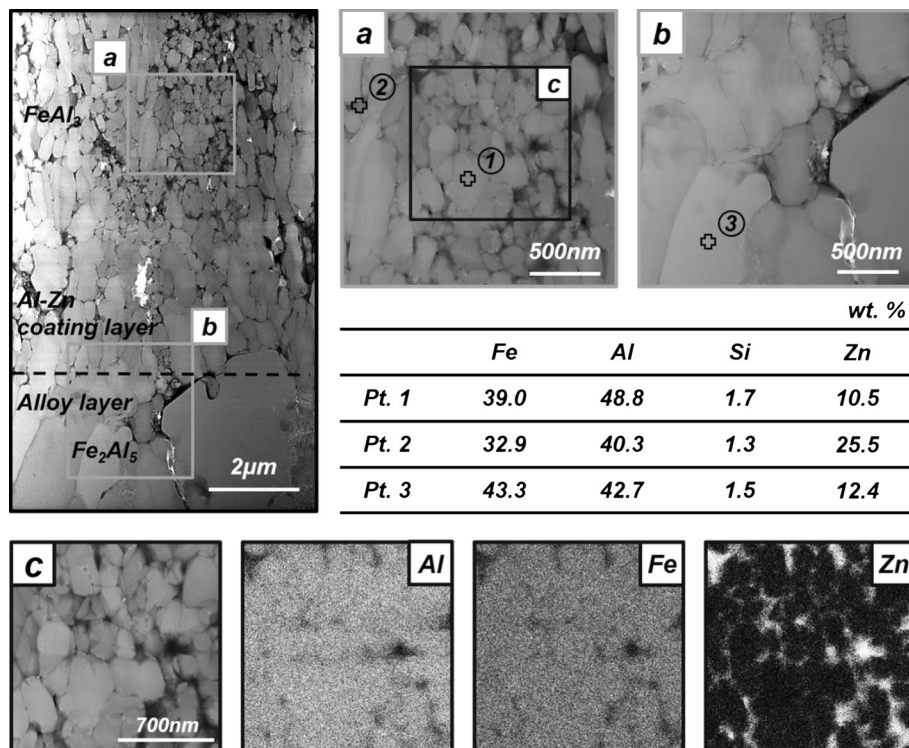


Fig. 5—(a, b) STEM image and corresponding elemental concentrations of the two selected areas in the image. (c) STEM image and corresponding elemental distribution for Al, Fe, and Zn in 55 wt pct Al-Zn coated 22MnB5 PHS heat treated at 1023 K (750 °C).

boundaries of the  $\text{Fe}_2\text{Al}_5$  intermetallic compounds, and (c) the cracks in the diffusion layer. It is very likely that the highly concentrated Zn in the diffusion layer is liquid at high temperatures and that it could cause LMIE, when press-forming stresses are applied, as this could result in the crack propagation into the steel matrix. Al-Si coatings on PHS show a similar tendency. In the case of the Al-10 pct Si coating on 22MnB5, the cracks present in the coating continuously propagate through the entire coating. The cracks, however, appear to stop in the diffusion layer. Chang *et al.*<sup>[20]</sup> reported that these cracks are cooling cracks, due to the difference in the

thermal expansion coefficient of the brittle  $\text{Fe}_2\text{Al}_5$  intermetallic and the steel substrate.

In the case of 55 wt pct Al-Zn coatings, the coating cracks are caused by a different mechanism. The cracks start as intergranular decohesion zones at the Fe-Al intermetallic grain boundaries covered with the Zn-rich phase and propagate to the diffusion layer. The cracks do not appear to propagate beyond the diffusion layer. These cracks are therefore due to the Zn which accumulated at  $\text{Fe}_2\text{Al}_5$  grain boundaries or at the interphase between the coating layer and the diffusion layer. The Zn-rich phase is liquid at the soaking and press-forming temperature and it may cause LMIE during press hardening. Zn-LMIE occurs when the two conditions are satisfied: (1) liquid Zn is in direct contact with the steel substrate and (2) a sufficiently high stress is applied.<sup>[21]</sup> In the present case, the steel had a fully austenitic microstructure (FCC) at temperatures higher than 1103 K (830 °C). Due to the Al diffusion into the steel substrate, the steel surface microstructure was changed to an ordered B2 FeAl intermetallic compound with a BCC crystal structure. This transformation resulted in a volume expansion which provided the required stress for localized LMIE to occur. The cracks did, however, not propagate beyond the diffusion layer into the matrix. This may be due to the fact that crack propagation in the ductile  $\alpha\text{-Fe(Al)}$  is more difficult than in the brittle FeAl phase.<sup>[11]</sup> The mechanism of LMIE by Zn accumulation and penetration is summarized in the schematic shown in Figure 9.

The soaking time and temperature were found to have an important influence on the microstructural evolution of the 55 wt pct Al-Zn coating during a press-hardening heat treatment. First of all, the coating microstructure was more stable at temperatures below 1083 K (810 °C). The coating had a compact structure without pores or coating cracks compared to the coating heat treated at 1173 K (900 °C). The Zn-rich phase remained clearly

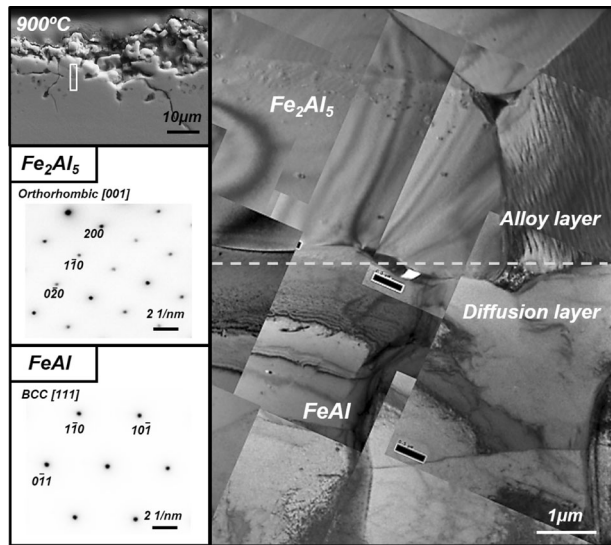


Fig. 6—TEM micrograph and corresponding selected area diffraction patterns for the  $\text{Fe}_2\text{Al}_5$  and FeAl intermetallic phases in 55 wt pct Al-Zn coated 22MnB5 PHS heat treated at 1173 K (900 °C).

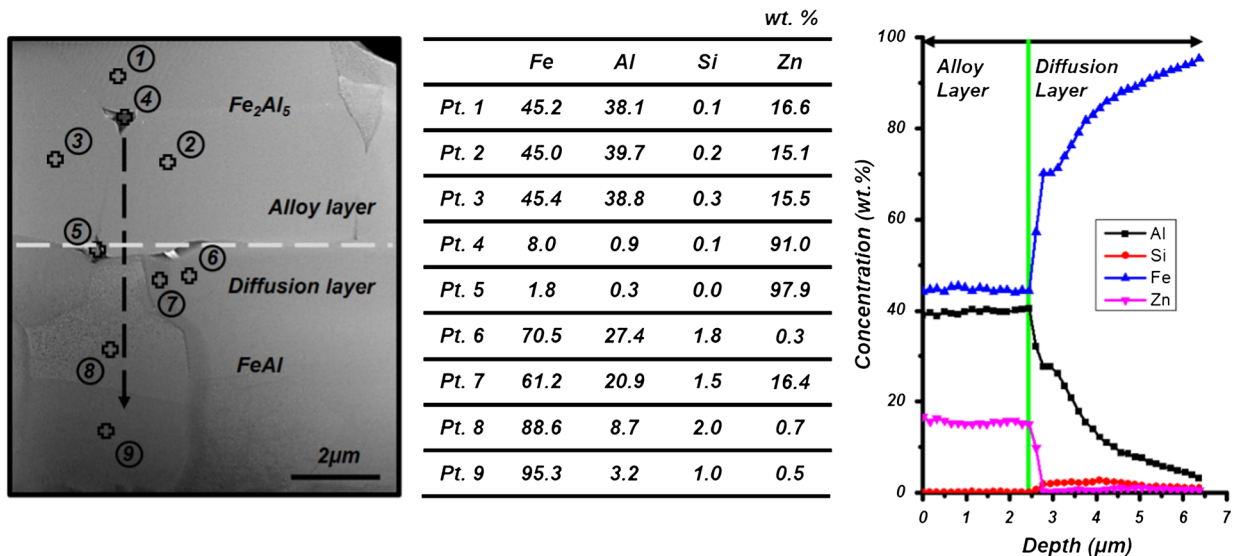


Fig. 7—STEM micrograph and elemental concentration for the numbered areas in the micrograph (left). Surface elemental depth distribution for Al, Si, Fe, and Zn for 55 wt pct Al-Zn coated 22MnB5 PHS heat treated at 1173 K (900 °C) (right).

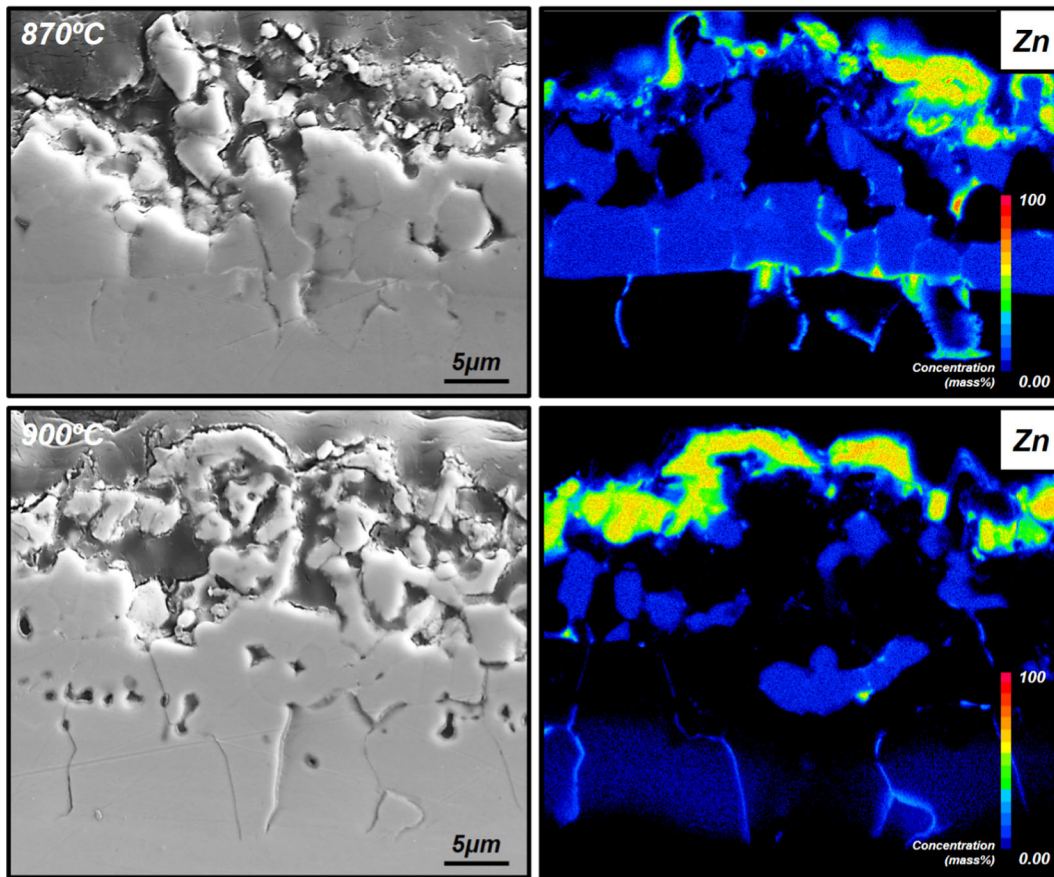


Fig. 8—Surface cross-sectional SEM images and corresponding Zn elemental distribution for 55 wt pct Al-Zn coated 22MnB5 PHS heat treated at 1143 K and 1173 K (870 °C and 900 °C).

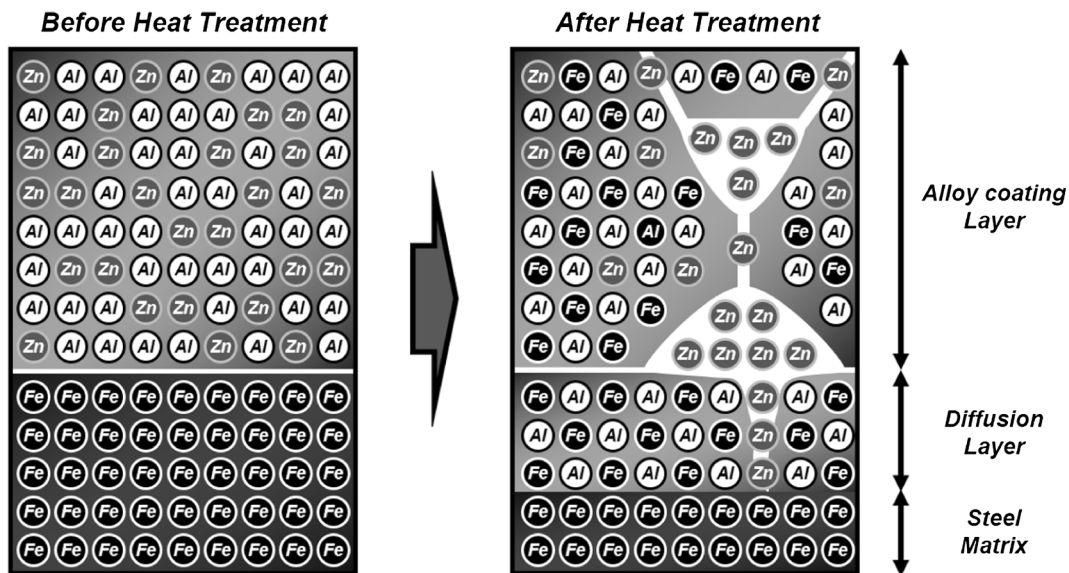


Fig. 9—Schematic of the mechanism of the accumulation of Zn between the grains of the Fe-Al intermetallic phases and the penetration of Zn in the grain boundaries of the diffusion layer during the press hardening heat treatment of 55 wt pct Al-Zn coated 22MnB5 PHS.

present between the grains of the  $\text{Fe}_2\text{Al}_5$  intermetallic. Figure 10 shows cross-sectional images and corresponding elemental distribution for Fe, Zn, and Al in a

specimen after heat treatment at the 1173 K (900 °C) for 4 and 8 minutes. When the heating time was reduced, the Fe-Al intermetallic compounds contained 15 wt pct



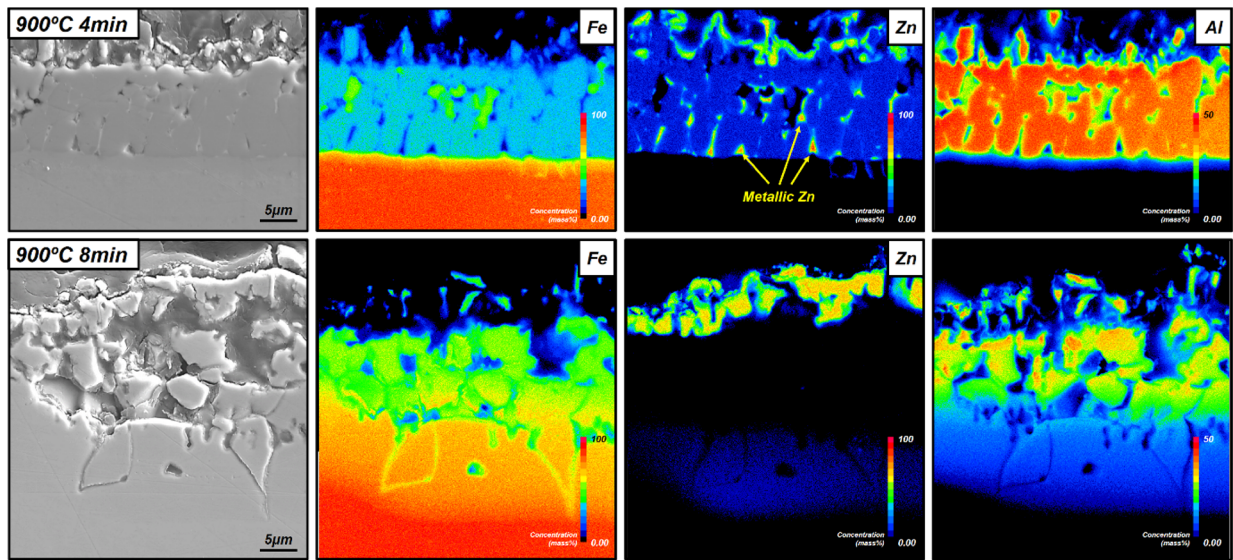


Fig. 10—Surface cross-sectional SEM images and corresponding elemental distribution for Fe, Zn, and Al for 55 wt pct Al-Zn coated 22MnB5 PHS heat treated at 1173 K (900 °C) for 4 and 8 min.

of Zn in solution. The Zn-accumulated region was also clearly visible at the grain boundaries between the  $\text{Fe}_2\text{Al}_5$  grains. As the diffusion layer was thin, no cracks occurred in this layer. However, when the soaking time increased, the coating initially broke into fragments, with Zn only forming ZnO layer at the top surface and the Zn being expelled to the grain boundaries in the intermetallic alloy layer. The diffusion layer contained less than 5 wt pct Zn. The observation implies that the Zn diffused into the FeAl phase during soaking. As the soaking time increased, the diffusion layer became thicker and the Zn enrichment of the boundaries resulted in inter-granular cracking. Fan *et al.*<sup>[11]</sup> reported that in Al-Si coated PHS heated at 1323 K (1050 °C) for 4 and 30 minutes, the Al-Si coating fully transformed to a disordered bcc  $\alpha$ -Fe with Al in solid solution. The diffusion of Al into the steel substrate of an Al-alloy coated PHS leads to the formation of Fe-Al intermetallic compounds such as FeAl or the solid solution  $\alpha$ -Fe(Al). The latter is a diffusion layer. Comparison of the two heat treatment times of 4 and 8 minutes indicates that a low heating temperature or a short soaking time is expected to be beneficial for Al-Zn coated PHS as it results in a better cathodic protection and improved coating stability.

A comparison of the electrochemical behavior for 55 wt pct Al-Zn and Zn coatings in a 3 pct NaCl solution is made in Figure 11 and Table II. The corrosion potential,  $E_{\text{corr}}$ , for the galvanized Zn coating before a PHS heat treatment was  $-1044.64$  mV. After being heat treated at 1173 K (900 °C), the coating layer was mainly composed of the  $\Gamma$  phase and  $\alpha$ -Fe(Zn). The fraction of  $\Gamma$  phase which has a higher Zn content than the  $\alpha$ -Fe(Zn) phase depends on the heating time. As the heating time increased, the  $\Gamma$  phase was eliminated and the Zn concentration of the coating decreased as a result of the Fe diffusion from the steel matrix into the coating.<sup>[14]</sup> Hence, after the heat treatment, the corro-

sion potential increased close to a value for the uncoated steel ( $-644.4$  mV), indicating that the heat-treated Zn coating does not provide cathodic protection in this condition. There were no large differences in the corrosion rate. The corrosion current density,  $I_{\text{corr}}$ , of the as-galvanized sample was  $27 \mu\text{A cm}^{-2}$  and after the heat treatment for 6 minutes, the room temperature corrosion current density of the sample was slightly increased to  $39 \mu\text{A cm}^{-2}$ . In contrast, Autengruber *et al.*<sup>[22]</sup> reported that after press hardening, the corrosion rate decreased due to lower potential differences. A passivation region was also clearly present in the polarization curve of the as-galvanized sample while after the heat treatment, the passivation region was absent. The passivation behavior may be caused by the formation of a thin continuous  $\text{Al}_2\text{O}_3$  layer at the surface.<sup>[18]</sup> However, after the heat treatment, the surface was almost entirely covered by ZnO, an oxide which does not provide a passivation effect.<sup>[22]</sup> The corrosion potential of 55 wt pct Al-Zn coating before the heat treatment was  $-1017.34$  mV. After heat treatment, the corrosion potential decreased slightly and became similar to the corrosion potential of the as-galvanized sample. An explanation for this is that the pure Zn regions in the coating layer contributed to the corrosion potential. It is clear that the Al-Zn coating provides a better cathodic protection than a pure Zn coating after press hardening. In addition, the passivation behavior of 55 wt pct Al-Zn coating after the press hardening heat treatment is shown. There is not much difference compared to the as-galvanized coating prior to press hardening.

## V. CONCLUSIONS

55 wt pct Al-Zn coated 22MnB5 PHS was given a thermal cycle corresponding to a press-hardening

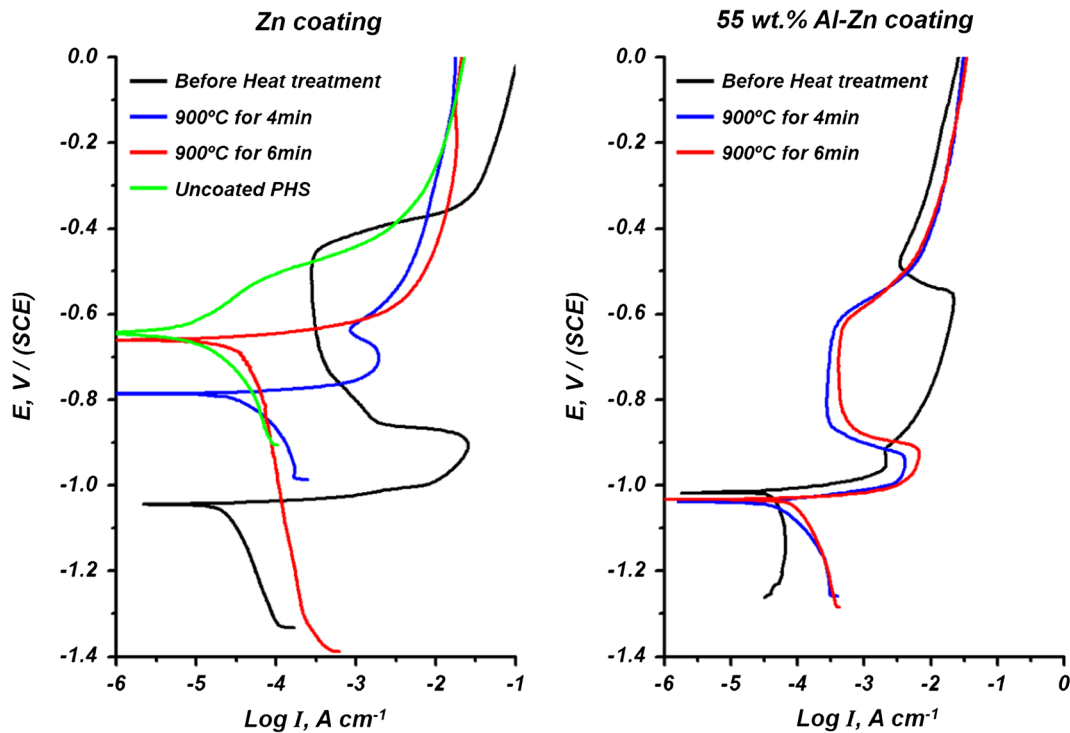


Fig. 11—Polarization curves for uncoated PHS, hot-dip Zn-coated PHS, and 55 wt pct Al-Zn coated PHS before and after a press hardening heat treatment. The tests were carried out at room temperature in a 3 pct NaCl solution.

Table II. Corrosion Parameters Obtained from the Electrochemical Polarization Curves

Samples	Zn Coating		55 Wt Pct Al-Zn Coating	
	$E_{\text{corr}}$ (mV-SCE)	$I_{\text{corr}}$ ( $\mu\text{A cm}^{-2}$ )	$E_{\text{corr}}$ (mV-SCE)	$I_{\text{corr}}$ ( $\mu\text{A cm}^{-2}$ )
Before heat treatment	-1044.64	26.83	-1017.34	42.96
Heating for 4 min	-786.09	36.72	-1038.51	46.04
Heating for 6 min	-661.26	39.13	-1032.99	89.38

process in order to evaluate the microstructure changes at the steel/coating interface. Fe was found to diffuse into the coating layer first and subsequently form Fe-Al intermetallic compounds. The coating layer was mainly composed of an intermetallic alloy layer ( $\text{Fe}_2\text{Al}_5$ ) and a diffusion layer ( $\text{FeAl}$ ,  $\alpha\text{-Fe}(\text{Al})$ ) at the end of this first stage.

In the second stage, the Zn was expelled from the intermetallic phases and accumulated at the grain boundaries of the Fe-Al intermetallic compounds. The high concentration of Zn between the grains of the Fe-Al intermetallic phase was found to be beneficial in terms of providing cathodic protection to the PHS. The sacrificial effect of the 55 wt pct Al-Zn coating was found to be much higher than that of a pure Zn coating after press hardening. This is due to the fact that after press hardening most of the surface of a Zn-coated PHS consists of  $\alpha\text{-Fe}(\text{Zn})$  with a low Zn concentration. The presence of a Zn-rich phase, formed during the press hardening of a 55 wt pct Al-Zn coated PHS, resulted in the penetration of Zn in the diffusion layer. In the case of press forming, this could potentially lead to a LMIE

fracture. The optimization of the soaking time and temperature is therefore key to the use of 55 wt pct Al-Zn coatings on the 22MnB5 PHS grade in industrial press hardening. The use of short soaking times and lower soaking temperature results in a coating with less pores and coating cracks, and minimizes the risk of LMIE for 55 wt pct Al-Zn coated 22MnB5 PHS.

#### ACKNOWLEDGMENTS

The authors gratefully acknowledge the support of Dr. Yeol Rae CHO of the POSCO Technical Research Laboratories in Gwangyang, South Korea.

#### REFERENCES

1. K. Steinhoff, N. Barbakadze, and M. Schupfer: *Galvatech 2011 conference*, Genova, Italy, 2011, pp. 319–26.
2. K.-P. Imlau, K.-J. Peters, and B. Schuhmacher: *Galvatech 2011 conference*, Genova, Italy, 2011, pp. 13–22.

3. J. Kondratiuk, P. Kuhn, E. Labrenz, and C. Bischoff: *Surf. Coat. Technol.*, 2011, vol. 205, pp. 4141–53.
4. K. Mori, K. Akita, and Y. Abe: *Int. J. Mach. Tools Manuf.*, 2007, vol. 47, pp. 321–25.
5. H. Karbasian and A.E. Tekkaya: *J. Mater. Process. Technol.*, 2010, vol. 210, pp. 2103–18.
6. C.-E. Ridderstråle, Patent GB1490535, Sweden, 1977.
7. H. Liu, X. Jin, H. Dong, and J. Shi: *Mater. Charact.*, 2011, vol. 62, pp. 223–27.
8. D.W. Fan, H.S. Kim, J.K. Oh, K.G. Chin, and B.C. De Cooman: *ISIJ Int.*, 2010, vol. 50, pp. 561–68.
9. F. Borsetto, A. Ghiotti, and S. Bruchi: *Key Eng. Mater.*, 2009, vols. 410–411, pp. 289–96.
10. D.W. Fan and B.C. De Cooman: *Steel Res. Int.*, 2012, vol. 83, pp. 412–33.
11. D.W. Fan and B.C. De Cooman: *ISIJ Int.*, 2010, vol. 50, pp. 1713–18.
12. C. Alléy, L. Dosdat, O. Clauzeau, K. Ogle, and P. Volovitch: *Surf. Coat. Technol.*, 2014, vol. 238, pp. 188–96.
13. C.W. Lee, D.W. Fan, S.J. Lee, I.R. Sohn, and B.C. De Cooman: *Proc. of GALVATECH 2011 Conf.*, Genova, Italy, 2011, pp. 327–34.
14. C.W. Lee, D.W. Fan, I.R. Sohn, S.J. Lee, and B.C. De Cooman: *Metall. Mater. Trans. A*, 2012, vol. 43A, pp. 5122–27.
15. P. Drillet, R. Grigorieva, G. Leuillier, and T. Vietoris: *8th International Conference on Zinc and Zinc Alloy Coated Steel Sheet*, Genova, Italy, 2011, pp. 371–78.
16. J. Federl: *1st International Conference on Hot Sheet Metal Forming of High-Performance Steel*, Kassel, Germany, 2008, pp. 283–91.
17. J.H. Selverian, M.R. Notis, and A.R. Marder: *J. Mater. Eng.*, 1987, vol. 9, pp. 133–40.
18. A.R. Marder: *Prog. Mater. Sci.*, 2000, vol. 45, pp. 191–271.
19. J.L. Murray: *Bull. Alloy Phase Diagr.*, 1983, vol. 4, pp. 55–73.
20. Y.Y. Chang, C.C. Tsaur, and J.C. Rock: *Surf. Coat. Technol.*, 2006, vol. 200, pp. 6588–93.
21. M.G. Nicholas and C.F. Old: *J. Mater. Sci.*, 1979, vol. 14, pp. 1–18.
22. R. Autengruber, G. Luckeneder, A.S. Kolnberger, J. Federl, and A.W. Hassel: *Steel Res. Int.*, 2012, vol. 83, pp. 1005–11.